Flame acceleration mechanisms to detonation in an obstacle-laden tube : Experiments and modelling

Kevin Cheevers[a], Hongxia Yang[a], Andrzej Pekalski[b] and Matei I. Radulescu[a]
[a] Department of Mechanical Engineering, University of Ottawa, Ottawa, Ontario, Canada
[b] Shell Global Solutions, Concord Business Park, Manchester, United Kingdom

1 Introduction

Predicting the acceleration of a flame through a congested geometry is an important problem in safety applications, which typically aim to prevent deflagration-to-detonation transitions (DDT). The acceleration process has been extensively studied in tubes with repeated obstructions (i.e. orifice plates or fence-type obstacles) [1]. The main role of these obstacles is to promote flame acceleration by introducing turbulence behind the bluff-body orifice plates which subsequently greatly deforms the flame. This process is well-visualized by Johansen & Ciccarelli, who injected helium ahead of the flame and tracked the motion of the helium as it was advected by the flow ahead of the flame and entrained into turbulent recirculation bubbles formed between adjacent obstacles [2].

The flame acceleration in tubes whose congestion comes in the form of repeated columns of small cylindrical obstacles, which is more representative of the obstruction provided by industrial piping, is less well understood. The experiments of Pinos & Ciccarelli shows the acceleration process of a hydrogen-air flame as it propagates through this type of congestion [3]. They focused on the acceleration in the low speed regime, observing multi-scale phenomena whose coupling between scales remains unclear, and the propagation of the high-speed detonation regime. However, there was no visualization of the high-speed deflagration immediately prior to the detonation transition as this occurred behind by a visually-opaque shock tube flange.

High-speed flame regimes remain poorly understood, being referred to as diffusionless fast flames [4] and ”strange wave” [5]. Maley suggested that auto-ignition plays an important role in creating local hot-spots, which then enhance the reactivity of the flame through mixing processes [6]. Others have attributed the high flame speeds as a result of high levels of turbulence which in turn increase the burning rate of the flame [7]. It is thus of interest to establish the propagation mechanism and structure of high speed flames immediately prior to DDT with adequately resolved visualization techniques.

The interaction of a high speed flame with a single obstacle was visualized by Rakotoarison [8]. They observed the main mechanism to be the enhancement of the burning rate resulting from flame deformation. The role of repeated obstacles and multi-scale effects were absent.

The current work studies the acceleration transient of a flame through a thin rectangular cross-sectioned tube congested by repeated columns of staggered cylindrical obstacles. A flame is ignited near the end of the shock tube which is filled with a premixed methane-oxygen or hydrogen-oxygen-nitrogen mixture.

Correspondence to: Kevin.Cheevers@uottawa.ca

The entire flame acceleration transient is visualized using high-speed photographic techniques, allowing time- and spatially-resolved observation of the flame structure's evolution. Most notably, the structure of the reactive wave immediately prior to the detonation transition is observed, as is the detonation transition itself, which were not previously visualized. A model is provided to recover the initial stages of flame acceleration, modelling the multi-scale physics governing the flame acceleration.

2 Experimental Method

The experiments were conducted in a shock tube with an overall length of 1.2 m and a rectangular cross section of 203 mm by 19 mm, as illustrated in Figure 1. Columns of cylindrical obstacles, each with a diameter of 25.4 mm and a thickness of 19 mm, are placed in the shock tube such that each column is also separated by one obstacle diameter. These obstacles impose a blockage ratio of 50%. A long wire ignition technique similar to Cheevers et al. was used to ignite a laminar flame near a tube extremity [9]. To shorten the ignition transient in the present sensitized mixtures, this wire was controlled using a MC002358 solid state relay and the voltage increased from 24 V to 48 V. The reactive mixtures were prepared beforehand using the method of partial pressures, after emptying the mixing tank to a pressure less than 40 Pa, and subsequently allowed to mix overnight prior to their use. The shock tube was emptied to a pressure less than 80 Pa prior each experiment. The two mixtures studied are CH_4+$2O_2$ at an initial pressure of 10.34 kPa and $2H_2$+O_2+$1.29N_2$ at an initial pressure of 18.96 kPa. The nitrogen dilution is added to the hydrogen mixture to lengthen the flame acceleration transient when compared to an undiluted hydrogen-oxygen mixture.

The experiments were visually monitored using a schlieren and shadowgraphy setup, the specifics of the latter being detailed elsewhere [9]. The Schlieren setup is implemented using a 1000 W Xenon Arc Lamp whose collimated light is converged onto a slit using a plano-convex lens with a focal length of 50 mm, prior to impinging onto the 305 mm-diameter parabolic mirrors. The light is cut-off using a thin blade placed at the focal length of the second mirror, then split into two components using a 50/50 beam splitter which are then directed towards two cameras, be it a Shimadzu HPV-X2 which records experiments with a high temporal resolution and limited spatial resolution, and a Phantom v1210 which records the experiments with a high spatial resolution and a limited temporal resolution. The exposure time of the two cameras are 200 ns and 468 ns, respectively. The cameras were triggered using a pressure sensor installed along the top wall near the field of view. The field of views of the Phantom encompassed the height of the shock tube, whereas the Shimadzu captured the flame propagation within a smaller field of view as illustrated in Figure 1.

3 Results

The shadowgraph visualization of a typical experiment conducted in stoichiometric methane-oxygen is shown in Figure 2. A flame is ignited along the tungsten wire, which preferentially grows along the height of the shock tube such that a finger flame propagates into the obstacles. As the flame progresses through the obstacles ($0.81 < t < 1.27$), one can follow the growth of individual finger flames in each pore, in addition to the growth of the macroscopic finger flame. As the small-scale fingers reach an obstacle, it splits into two smaller fingers to circumvent the obstacle, and repeat this process upon reaching subsequent columns. The flame acceleration in the left-hand columns of Figure 2 is dominated by the growth and propagation of the small-scale flame fingers which feeds back into the growth of the macroscopic finger flame occupying the height of the tube. The amplitude of the macroscopic finger is seen to grow over time as the flame tip propagates further into the obstacle grid whereas the tails of the flame skirt remain in the close vicinity of the ignition wire and never enters the obstacle grid. The

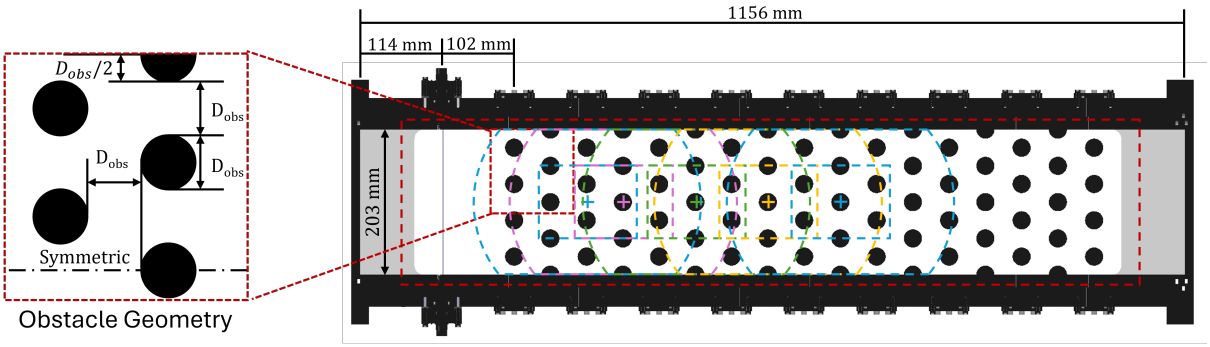

Figure 1: Illustration of the experimental apparatus. The thickness of the channel in the third dimension is 19 mm. The obstacles have a diameter of $D_{obs} = 25.4$ mm, which controls the geometry of the staggered obstacles. The Shadowgraph field of view is illustrated in red, whereas the schlieren fields of view are shown in various colours.

growth of the amplitude of the fingers at various scales continues until around 1.4 ms, at which point a second distinct structure appears comprised of a series of shock waves which are closely followed by a highly textured flame. This structure is exemplified in the frames taken at a time of $t = 1.44 - 1.49$ ms. Finally, a transition to detonation occurs in the following frame near the top of the tube.

The propagation speed of the leading edge of the reaction wave is shown in Figure 3 for experiments in both mixtures. The flame propagating through the hydrogen mixture, whose chemistry results in a higher sensitivity to shock-induced autoignition, accelerates until reaching a velocity on the order of 1000 m/s. At this point, a sudden increase in flame speed is linked to the detonation transition. In contrast, the methane flame exhibits a continuous acceleration from the ignition of the flame until attaining a speed on the order of the CJ detonation speed ($\sim$ 2300 m/s), with no visible point where a distinct regime transition occurs. Flame speed oscillations are linked with the periodic acceleration and deceleration of the flow within the vicinity of obstacles.

Spatially-resolved schlieren images of the flame acceleration process are shown in Figure 4. A cellular flame enters the obstacles near the centre of the channel in the first image. As a result of the flame acceleration, rightward-propagating shocks appear ahead of the flame. These shocks reflect off the obstacles and re-interact with the flame, which burns faster and drive additional compression waves which then also reflect off the obstacles. These shock reflections result in the complex shock structure seen around column 5 in the methane mixture, and column 8 in the hydrogen mixture. The flame in these structures is strongly deformed by its entrainment through vortices behind the obstacle and Richtmyer-Meshkov instabilities resulting from multiple shock-flame interactions. This structure eventually transits to a detonation, which appears as the much thinner structure as identified in the final frames. The structure of the wave below the detonation remains a shock-flame complex until the passage of the detonation through those pores.

Figure 5 shows selected time-resolved images of the high-speed flame structure immediately prior to its transition to detonation, recorded using a framing rate of 1 million frames per second. In both mixtures, multiple shocks followed by a flame enter the left-hand side of the first image. This structure survives the reflection of the shocks off the first obstacle, which then re-interact with and subsequently enhances the flame. The flame is then propelled through the pore. The second shock reflection in the hydrogen mixture, shown in the top right image, results in a sudden transition to a faster reactive wave. This thinner detonation wave then wraps around the obstacle and propagates ahead of the shock-flame complex, in addition to consuming the unreacted gas between the shock and the flame as it propagates transversely. In contrast to this sudden transition between regimes, the methane flame enters the first

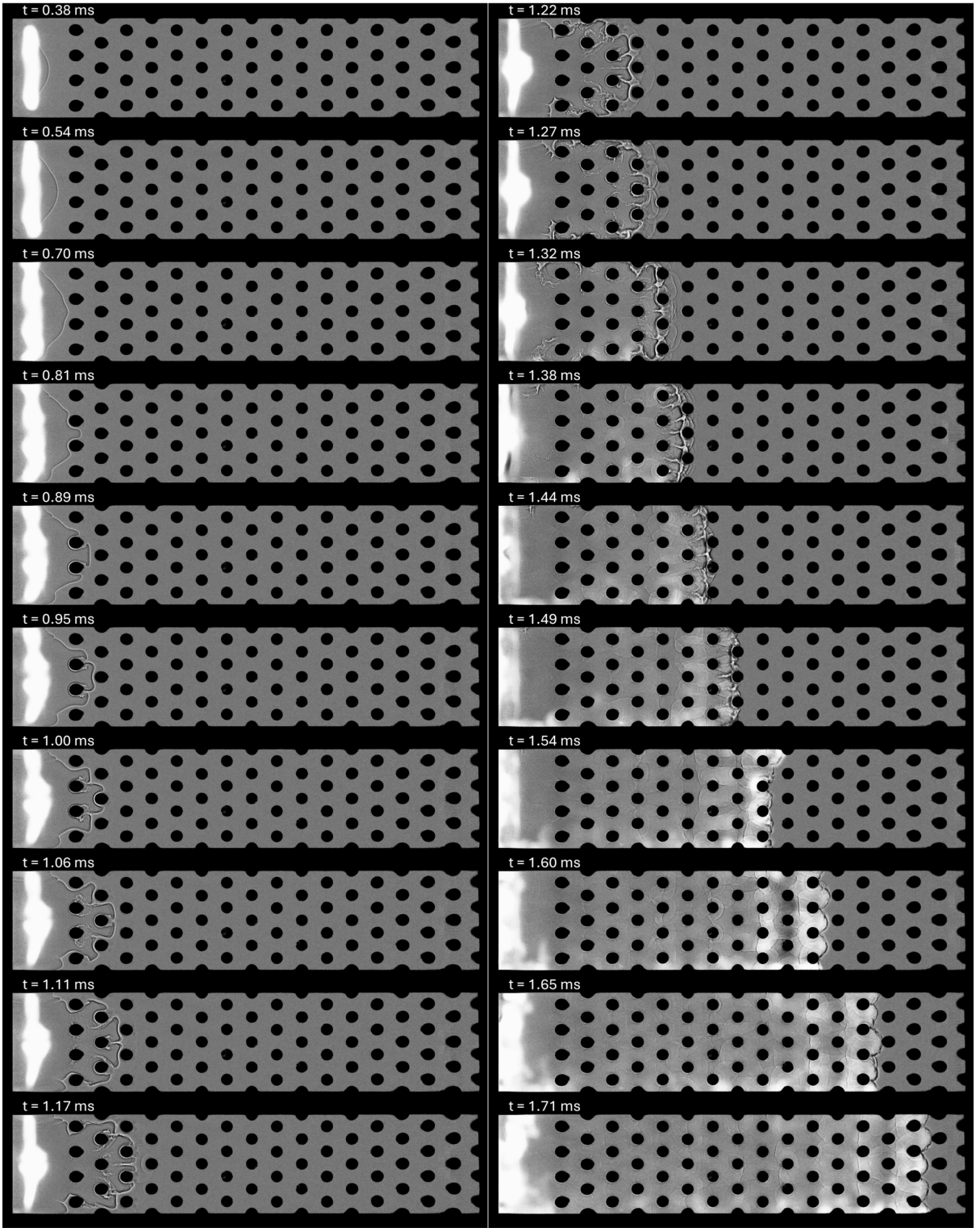

Figure 2: Shadowgraph visualization of the propagation of a stoichiometric methane-oxygen flame ignited near the left end of the tube, at an initial pressure of 10.34 kPa.

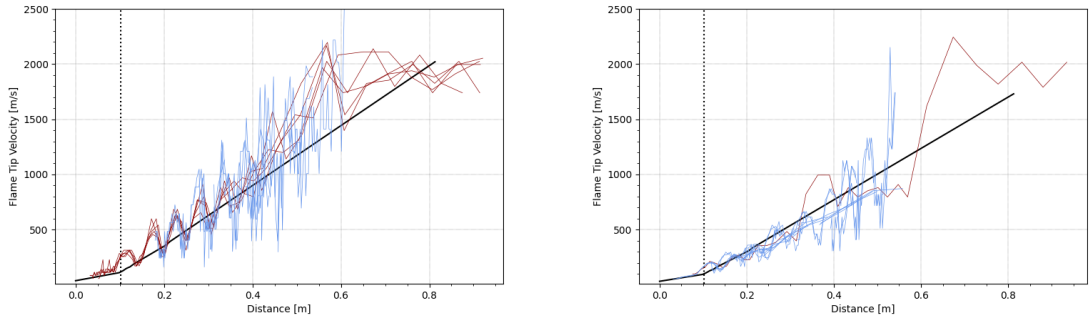

(a) $CH_4 + 2O_2$ (b) $2H_2 + O_2 + 1.29N_2$

Figure 3: Spatial evolution of the flame tip velocity (x_f). Measurements made from shadowgraph images are shown in red, whereas those made from schlieren visualization are shown in blue. The flame speed predicted by the embedded finger flame model is shown in black.

field of view shown in the lefthand column with a speed around 1200 m/s, and continuously accelerates through the field of view. As it approaches the tenth column of obstacles, its speed has increased to around 1900 m/s. Despite these high speeds, approaching the CJ detonation speed of 2300 m/s at the quiescent conditions, the flame still appears to consume gases via diffusively-controlled processes, as opposed to through autoignition of gases behind the lead shocks. Once the lead shock reflects off the tenth column of obstacles, a detonation forms and is transmitted through the remainder of the reactants.

4 Embedded Finger Flame Model

Recalling the experiments presented above, a feature which is apparent at early times is the growth of the finger flame at an outer scale which is governed by the height of the channel, and the growth of smaller-scale fingers at an inner scale as they periodically jet through gaps in successive columns of obstacles. This is modelled as a multi-scale problem, in which the growth of the surface area at the outer scale and inner scales are coupled, essentially embedding small flame fingers onto a larger finger flame. From this point of view, the evolution of the speed of the flame tip is dictated by the growth of the large-scale finger flame, where smaller-scale fingers whose growth is dictated by the large scale flame add a significant fractal-like contribution to the flame surface area. An important aspect appearing in this model is the fundamental coupling between scales, which may be of interest for sub-grid modelling.

The model is derived under the assumptions of elliptical flame fingers, constant laminar burning velocity, and constant fresh and product gas densities while neglecting flame stretch and compressibility effects. The final equation describing the acceleration of the flame is given by

$$\frac{dx_f}{dt} = \frac{\sigma S_L}{H}\left[(x_f + H) + \left(\frac{x_f - X_{obs}}{X_{obs}}\mathcal{H}(X_{obs} - x_f) + 1\right)H + \sum_i \mathcal{H}(x_i - X_{obs})(x_i - X_{obs} + h)\right], \tag{1}$$

in which the bracketed term is the growth of the flame's surface area. The first term models the growth of the macroscopic flame finger, the second corrects for the presence of a leftwards propagating flame in experiments, whereas the third term models the growth of the small flame fingers embedded onto the macroscopic flame as it propagates through each pore. This model recovers the initial stages of flame acceleration from the initial ignition until compressibility effects become important, as seen in Figure 3. However, these effects become very important around the speed at which the coupled shock-

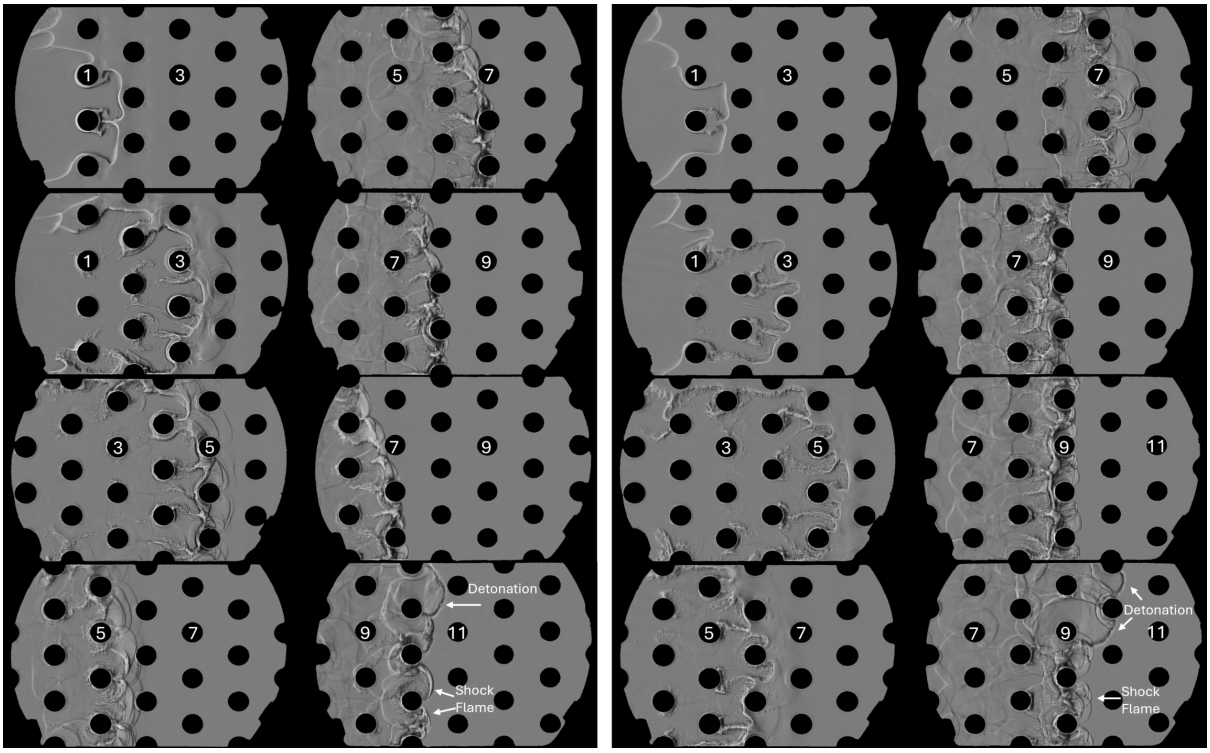

Figure 4: Spatially-resolved schlieren images of the flame acceleration process in (left) CH_4+$2O_2$, and (right) $2H_2$-O_2-$1.29N_2$. The number of obstacle columns are numbered.

flame structure appears, which accelerates as a result of different physics and is thus not expected to be recovered by this model.

5 Concluding Remarks

The present work presents highly-resolved visualization of the flame acceleration process in a tube obstructed by staggered cylindrical obstacles. At early times, the flame grows as a multi-scale finger flame whose macroscopic scale is dictated by the dimensions of the tube and whose smaller-scales appear as a result of the flame jetting through pores between the obstacles. A model embedding small-scale fingers onto a macroscopic finger and coupling these two scales together predicts the acceleration of the flame in this first regime.

Once the flame sufficiently accelerates for compressibility effects to become important, shocks appear ahead of the flame and reflect off obstacles, re-interacting with the flame and depositing significant amounts of vorticity in the flow. The flame acceleration mechanism changes in this high-speed regime, and is thus not expected to be recovered by the embedded finger flame model. In the hydrogen mixture, which is more sensitive to shock-induced autoignition, the reflection of the lead shock off an obstacle when the flame tip propagates around 1000 m/s results in a sudden transition to a detonation, which outruns the flame due to its higher propagation speed. However, in the methane mixture which is less sensitive to autoignition, a progressive acceleration of this high speed flame occurs from 1000 m/s to 2000 m/s. The structure of the fast flame during this acceleration is resolved, and the fresh gas appears to be consumed through diffusive processes throughout this transient. Once the flame accelerates to around 2000 m/s, a detonation appears as a third distinct regime.

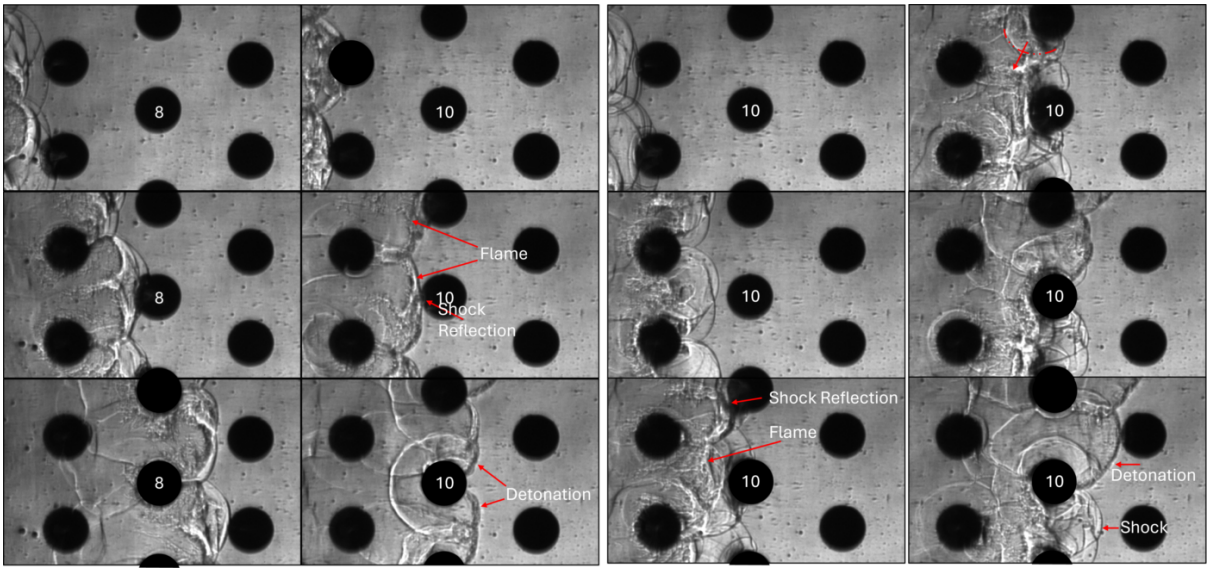

Figure 5: Time-resolved schlieren images of the flame structure immediately prior to detonation transition (left) CH_4+2O_2, and (right) 2H_2-O_2-1.29N_2. The number of obstacle columns are numbered.

References

[1] G. Ciccarelli and S. Dorofeev, "Flame acceleration and transition to detonation in ducts," *Progress in Energy and Combustion Science*, vol. 34, no. 4, pp. 499–550, 2008.

[2] C. T. Johansen and G. Ciccarelli, "Visualization of the unburned gas flow field ahead of an accelerating flame in an obstructed square channel," *Combustion and Flame*, vol. 156, no. 2, pp. 405–416, 2009.

[3] T. Pinos and G. Ciccarelli, "Combustion wave propagation through a bank of cross-flow cylinders," *Combustion and Flame*, vol. 162, no. 9, pp. 3254–3262, 2015.

[4] J. F. Clarke and N. Nikiforakis, "Remarks on diffusionless combustion," *Philosophical Transactions of the Royal Society of London. Series A: Mathematical, Physical and Engineering Sciences*, vol. 357, no. 1764, pp. 3605–3620, 1999.

[5] A. Khokhlov, E. Oran, and G. Thomas, "Numerical simulation of deflagration-to-detonation transition: the role of shock–flame interactions in turbulent flames," *Combustion and Flame*, vol. 117, no. 1, pp. 323–339, 1999.

[6] L. Maley, R. Bhattacharjee, S.-M. Lau-Chapdelaine, and M. Radulescu, "Influence of hydrodynamic instabilities on the propagation mechanism of fast flames," *Proceedings of the Combustion Institute*, vol. 35, no. 2, pp. 2117–2126, 2015.

[7] A. Y. Poludnenko, T. A. Gardiner, and E. S. Oran, "Spontaneous transition of turbulent flames to detonations in unconfined media," *Physical Review Letters*, vol. 107, no. 5, p. 054501, 2011.

[8] W. Rakotoarison, B. Maxwell, A. Pekalski, and M. I. Radulescu, "Mechanism of flame acceleration and detonation transition from the interaction of a supersonic turbulent flame with an obstruction: Experiments in low pressure propane–oxygen mixtures," *Proceedings of the Combustion Institute*, vol. 37, no. 3, pp. 3713–3721, 2019.

[9] K. Cheevers, H. Yang, A. Pekalski, and M. I. Radulescu, "The deformation of h2-air flames from head on interactions with expansion waves," *Proceedings of the Combustion Institute*, 2024.